

Structural properties of liquid alkali-metal–lead alloys: NaPb, KPb, RbPb, and CsPb

H. T. J. Reijers,* M.-L. Saboungi, D. L. Price, J. W. Richardson, Jr., and K. J. Volin
 Argonne National Laboratory, 9700 South Cass Avenue, Argonne, Illinois 60439

W. van der Lugt

Solid State Physics Laboratory, University of Groningen, 9718 EP Groningen, Melkweg 1, The Netherlands
 (Received 16 May 1989)

The structural properties of liquid equiatomic alkali-metal–lead alloys APb , with $A = Na, K, Rb,$ and Cs , have been studied with neutron diffraction. The experimental data are reduced to the neutron-weighted total structure factors $S(Q)$ and radial distribution functions $n(r)$. In all the systems studied, $S(Q)$ is characterized by a first sharp diffraction peak (FSDP) at $Q \sim 1 \text{ \AA}^{-1}$ and $n(r)$ by structure in the first coordination shell at $r = 3\text{--}4 \text{ \AA}$, both features indicating the presence of polyatomic structural units. Two types of structural models have been fitted to the experimental data, both based on consideration of such units: the random packing of structural units model, and the reference interaction site model. The structures of the units are derived from powder-diffraction measurements made with the same instrument on solid polycrystalline samples. Allowing for a slight expansion of the units on melting and using physically reasonable values for the adjustable parameters, both models give satisfactory agreement with the experimental data and are used to give the partial structure factors and pair distribution functions. Inelastic-scattering measurements have been made on one system, liquid KPb, using a spectrometer at the same source. These yield a value for the mean diffusion constant, $D = 1.2 \pm 0.2 \times 10^{-5} \text{ cm}^2/\text{sec}$, and a smoothly varying inelastic scattering spectrum with no indication of excitations of a molecular character. The FSDP remains well defined when the inelastic scattering is integrated over small energy transfers, indicating a lifetime of 10^{-13} sec or longer for the intermediate-range order responsible for this peak.

I. INTRODUCTION

A recent investigation of the structure of liquid equiatomic KPb by two different groups^{1,2} revealed the presence of a first sharp diffraction peak (FSDP) in the total structure factor $S(Q)$ at low wave vector, $Q \sim 1 \text{ \AA}^{-1}$. The FSDP was interpreted as a clear manifestation of the existence of K_4Pb_4 structural units in the liquid; the atomic structure of these units was assumed to be similar to that reported in the corresponding intermetallic solid, consisting of nearly regular Pb_4 tetrahedra surrounded by K_4 tetrahedra oriented in the opposite direction.²

The electrical^{3,4} and thermodynamic^{5–8} properties of these liquid alloys have interesting features that can be summarized as follows. In the Na-Pb system, the electrical resistivity as a function of alloy composition reaches a maximum of $445 \mu\Omega \text{ cm}$ at Na_4Pb , and a small shoulder of $290 \mu\Omega \text{ cm}$ is reported at NaPb;⁵ the excess stability shows maxima⁵ at both compositions, but the excess heat capacity of NaPb is small and has a negligible temperature dependence.⁶ In the K-Pb, Rb-Pb, and Cs-Pb alloys, only one maximum is reported in the electrical resistivity at the equiatomic composition with typically nonmetallic values, e.g., $7000 \mu\Omega \text{ cm}$ for CsPb with a large negative temperature coefficient, $-115 \mu\Omega \text{ cm K}^{-1}$.³ The excess stability for K-Pb (Ref. 7) and Rb-Pb (Ref. 8) exhibits one maximum at the equiatomic composition, while the excess heat capacity for KPb, RbPb, and CsPb increases with decreasing temperature, reaching unusually large values in the vicinity of the melting point.⁶

The objective of our study was to investigate the structure of these alloys in the liquid and solid states. The aim was to detect anomalies or signatures, if any, in the structure to explain the electrical and thermodynamic properties. The crystalline structures were also determined, since they could have direct implications on the interpretation of the liquid structure, as was the case in our previous work on liquid KPb.² Several questions are needed to be addressed, e.g., what are the structural differences between NaPb on the one hand and KPb, RbPb, and CsPb on the other? Does the Zintl ion, Pb_4^{4-} , present in the solid⁹ survive the melting process in these alkali-metal–lead alloys?

In this paper, we report results of neutron-diffraction experiments on liquid and polycrystalline NaPb, RbPb, and CsPb and on polycrystalline KPb carried out at the Special Environment Power Diffractometer¹⁰ (SEPD) at the Intense Pulsed Neutron Source (IPNS) of Argonne National Laboratory. The atomic structures of the crystalline materials were derived by standard Rietveld analysis. Structure factors obtained for the liquid phase were analyzed in terms of structural units deduced from the crystalline structures.

The presence of structural units of the form A_4Pb_4 , indicated by the present neutron-diffraction results and thermodynamic measurements,^{5–8} suggested the possibility of observing the internal vibrations of these units spectroscopically. Because of the high conductivity, inelastic neutron scattering appeared to be a more promising approach than optical spectroscopy. A recent mea-

surement¹¹ of this kind on vitreous GeSe₂ glass revealed the four characteristic vibrational frequencies of the Ge(Se_{1/2})₄ tetrahedra that make up the network of this glass. Measurements on KPb at room temperature and slightly above the melting point were carried out at the Low Resolution Medium-Energy Chopper Spectrometer¹² (LRMECS) at IPNS.

In the following, we report the information obtained about the structure of these alloys and identify correlations between the electrical and thermodynamic properties and the structural data.

II. EXPERIMENTS

A. Neutron-diffraction measurements

Thin-walled vanadium crucibles (about 0.02 cm) with an internal diameter of 0.64 cm and a height of 6.35 cm were used as containers. They were first fired at $\sim 800^\circ\text{C}$ in high vacuum to eliminate any oxide coating on the surface. Equiatomic alloys were taken from the contents of capsules used earlier for a heat-capacity determination by drop calorimetry,⁶ were crushed, and were loaded into the vanadium crucibles inside a high-purity, helium-filled glovebox. The amounts were carefully weighed and controlled to ensure a height of at least 5 cm in the liquid state. This procedure was followed for two reasons. First, when we attempted to load the alkali metal and lead directly into the vanadium crucibles, the thin walls were distorted upon heating, presumably due to the changes accompanying the formation of the alloys. Such reaction did not occur when the thin-walled crucibles were loaded with already-formed equiatomic alloys, such as those used in the calorimetric measurements.⁶ Second, the use of the same materials could present considerable advantages in correlating results obtained in different experiments. An empty crucible with the same dimensions were similarly prepared and used to measure the contribution of the container scattering. All vanadium crucibles were hermetically sealed using electron-beam welding.

Time-of-flight (TOF) diffraction measurements were carried out at SEPD. The crucible was mounted in a high-temperature, vanadium-foil vacuum furnace. Sample temperatures were monitored with a thermocouple located in the pedestal base supporting the crucible and in close contact with it. Polaroid film exposures were made with a neutron camera to ensure that the sample was centered in the incident beam, which was collimated to a 5-cm height and a 1-cm width. Data were collected simultaneously in eight separate groups of detectors positioned about scattering angles of $\pm 150^\circ$, $\pm 90^\circ$, $\pm 60^\circ$, $+30^\circ$, and -15° with respect to the incident beam. A measurement was first made in the solid phase and analyzed using the Rietveld refinement technique; the sample was then heated and measurements of the liquid were carried out in the vicinity of the melting point. For background subtraction, measurements of the empty crucible were made at an average temperature of 900 K. For purposes of instrument calibration and data normalization, measurements were also made with a 0.64-cm-diam vanadium standard and with the spectrometer empty, both at room temperature.

B. Inelastic-scattering measurements

Inelastic-scattering measurements were made on KPb in both solid (300 K) and liquid (870 K) phases. The sample was encapsulated in a vanadium tube 1.11 cm in diameter, with the KPb sample covering the full height of the LRMECS beam, 10.16 cm. The sample was installed in a furnace used in an earlier measurement¹³ on molten RbBr, consisting of a spiral tantalum wire around the sample and a molybdenum radiation shield. The liquid temperature was maintained at 870 ± 10 K. Runs were made with the solid and liquid samples and an equivalent empty container. An incident energy of 50.7 meV was used, and the scattering was observed in 32 groups of detectors spanning scattering angles ϕ from 2.4° to 116.7° . The energy transfer $E = E_0 - E_1$, where E_0 and E_1 are the incident and scattered energies, was obtained from time-of-flight analysis of the scattered neutrons.

The detector groups were normalized by means of an independent measurement on a room-temperature vanadium sample. Data were analyzed using standard programs.¹⁴ The resolution function of the spectrometer was calculated with an analytical procedure. It has a full width at half maximum of 2.8 meV and a slightly asymmetrical shape, with a tail extending toward the negative E side, reflecting the asymmetry of the source pulse as a function of time. Multiple scattering was not corrected for but was estimated to be on the order of 10% of the primary scattering.

C. Results and discussion

1. Determination of the crystal structures

The room-temperature x-ray crystal structure of NaPb was first reported in 1953 by Marsh and Shoemaker.¹⁵ Hewaidy, Busmann, and Klemm¹⁶ found KPb, RbPb, and CsPb to be isostructural with NaPb, based on analysis of x-ray-diffraction powder patterns. No further structural details were obtained. NaPb crystallizes in the tetragonal space group $I4_1/acd$, with 32 formula units per unit cell. In this structure, the Pb atoms lie on general positions forming nearly regular Pb₄ tetrahedra. There are two crystallographically distinct Na atom sites, Na(1) at special positions equivalent to $(x, 0, \frac{1}{4})$ and Na(2) at positions $(y, \frac{1}{4} - y, \frac{1}{8})$. Marsh and Shoemaker¹⁵ approximated the Na atomic parameters x and y as 0.375. The precision of these parameters were poor, since the x-ray scattering amplitude of Na is only about $\frac{1}{9}$ that of Pb.

The coherent neutron-scattering length for Pb is 9.405 fm; these lengths for Na, K, Rb, and Cs are 3.63, 3.71, 7.08, and 5.42 fm, respectively.¹⁷ Thus, the neutron-scattering lengths of Na and Pb are within a factor of 3, much closer than the x-ray scattering amplitudes. The scattering length of K is similar to that of Na, while Rb and Cs are relatively strong scatterers. As a result, our neutron-diffraction refinements can be expected to produce high-precision structural data for all atoms.

Data from the $\pm 150^\circ$ data banks for NaPb at 570 K and KPb, RbPb, and CsPb at room temperature were analyzed with the Rietveld refinement technique modified

for use with TOF data from a pulsed neutron source.¹⁸ Conventional background scattering data were fitted with a six-parameter analytical function.^{19,20} The range of reciprocal space analyzed in each case was 0.86–3.97 Å⁻¹. The final Rietveld refinement parameters are presented in Table I, along with the parameters of Marsh and Shoemaker for NaPb at room temperature.¹⁵ Measured solid densities are from Hewaidy *et al.*¹⁶

All structures are refined satisfactorily with the $I4_1/acd$ space group reported by Marsh and Shoemaker.¹⁵ They can be described in terms of the coordination of A atoms ($A = \text{Na, K, Rb, and Cs}$) around the Pb_4 tetrahedra. The closest shell consists of four $A(1)$ atoms situated opposite the faces of the Pb_4 tetrahedron, forming a larger tetrahedron oriented in the opposite direction. The second shell consists of four $A(2)$ atoms located at the corners of a square opposite the edges of the Pb_4 tetrahedron. All of these A atoms are shared by two neighboring Pb_4 tetrahedra.

Considering now the coordination about individual atoms, each Pb atom has three nearest neighbors, the other atoms in the Pb_4 tetrahedron, and seven neighboring A atoms [four $A(1)$ and three $A(2)$]. Each A atom has, on average, seven nearest-neighbor Pb atoms and four to five neighboring A atoms. The latter are further away than the Pb atoms, but less so for the heavier alkali metals.

A comparison of the neutron-diffraction results for NaPb at 570 K with the x-ray results at 295 K shows measurable but minor differences. The neutron results are clearly of higher precision, primarily due to the smaller scattering contrast between Na and Pb. Moreover, the positional parameters of Na(1) and Na(2) deviate from the estimates of Marsh and Shoemaker by about 5–6 times the estimated (Rietveld refinement) error. In most other respects, the x-ray results are very representative of the more precise neutron results.

Lattice parameters for the remaining materials follow

TABLE I. Crystallographic data for NaPb, KPb, RbPb, and CsPb.

	NaPb ^a RT	NaPb 570 K	KPb RT	RbPb RT	CsPb RT
a_0	10.580(5)	10.7197(1)	11.5372(1)	11.8986(1)	12.2561(1)
c_0	17.746(15)	17.8617(3)	18.8698(2)	19.4406(3)	20.0238(4)
$V, \text{Å}^3$	1986.42	2052.50(5)	2511.70(3)	2752.32(4)	3007.80(6)
$\rho_m (\text{g cm}^{-3})$	6.18		5.20	5.59	5.92
$\rho_x (\text{g cm}^{-3})$	6.16	5.96	5.21	5.65	6.01
$A(1),^b x$	0.375	0.3811(9)	0.3682(4)	0.3626(3)	0.3576(4)
$A(2),^c x$	0.375	0.3715(7)	0.3771(2)	0.3800(2)	0.3802(3)
Pb, x	0.0696(13)	0.0667(2)	0.0618(1)	0.0616(2)	0.0610(2)
Pb, y	0.1186(12)	0.1187(2)	0.1301(1)	0.1350(1)	0.1404(2)
Pb, z	0.9383(8)	0.9378(2)	0.9335(1)	0.9312(1)	0.9297(1)
Pb-Pb, $2X$	3.162(20)	3.166(4)	3.118(2)	3.098(3)	3.086(3)
Pb-Pb, $1X$	3.146(20)	3.158(5)	3.113(2)	3.105(3)	3.074(4)
Pb-Pb, $1X$	3.642(20)	3.668(4)	4.164(2)	4.430(3)	4.691(4)
$A(1)$ -Pb, $2X$	3.39(10)	3.502(7)	3.807(4)	3.936(3)	4.073(5)
$A(1)$ -Pb, $2X$	3.49(10)	3.505(8)	3.838(4)	3.979(3)	4.109(5)
$A(1)$ -Pb, $2X$	3.56(10)	3.575(2)	3.812(1)	3.951(2)	4.083(2)
$A(1)$ -Pb, $2X$	3.62(10)	3.631(3)	3.860(1)	3.975(2)	4.112(2)
$A(2)$ -Pb, $2X$	3.36(10)	3.408(3)	3.682(1)	3.832(2)	3.978(2)
$A(2)$ -Pb, $2X$	3.42(10)	3.455(7)	3.802(3)	3.944(3)	4.064(4)
$A(2)$ -Pb, $2X$	3.48(10)	3.502(2)	3.816(1)	3.975(2)	4.136(2)
$A(1)$ - $A(2)$, $2X$	3.70(10)	3.703(7)	4.044(4)	4.204(3)	4.375(4)
$A(1)$ - $A(2)$, $2X$	3.70(10)	3.744(10)	3.965(4)	4.079(4)	4.160(5)
$A(2)$ - $A(2)$, $1X$	3.74(10)	3.895(20)	4.011(8)	4.037(6)	4.154(10)
$R_F^2,^d \%$		11.7	9.0	7.9	7.7
$R_{wp},^e \%$		5.3	5.0	5.2	5.4
$R_{\text{expt}},^f \%$		4.7	3.4	4.4	4.8

^aX-ray structure of Marsh and Shoemaker (Ref. 15).

^b $A(1)$ corresponds to Na(1), K(1), Rb(1), Cs(1).

^c $A(2)$ corresponds to Na(2), K(2), Rb(2), Cs(2).

^d $R_F^2 = 100.0 \times \{ \sum [|I(\text{obs}) - I(\text{calc})|] / \sum |I(\text{obs})| \}$.

^e $R_{wp} = 100.0 \times \{ \sum W \times [Y(\text{obs}) - Y(\text{calc})]^2 \}^{1/2} / \{ \sum Y(\text{obs})^2 \}^{1/2}$. $W(\text{TOF})$ is weight, and $Y(\text{TOF})$ is neutron counts.

^f $R_{\text{expt}} = 100.0 [N / \sum W \times Y(\text{obs})^2]^{1/2}$, where N is the number of degrees of freedom.

the expected trend: increasing in the order NaPb→KPb→RbPb→CsPb. A -Pb and A - A distances and the separation between Pb_4 tetrahedra follow similar trends, although there is a 0.10–0.20-Å spread in first-neighbor distances. The sizes (edge lengths) of the Pb_4 tetrahedra are apparently governed by the alkali-metal packing arrangement, which decreases systematically in the order NaPb→KPb→RbPb→CsPb.

Anisotropic Debye-Waller factors are presented in Table II. The values for NaPb at 570 K are higher than those for KPb, RbPb, and CsPb at room temperature, as expected. Anisotropies are observed for NaPb and KPb, which may be due to preferred orientation in the material, although the values obtained were not affected by a preferred orientation correction.

All refinements revealed thermal diffuse scattering components slowly oscillating about the baselines of the crystalline patterns; they were removed using a Fourier-filtering technique.²¹

2. Determination of the liquid structure

The liquid-phase data were analyzed with standard procedures developed at Argonne National Laboratory for glass and liquid diffraction data, incorporating simple corrections for multiple scattering and inelasticity effects. Data from the detector groups at $\pm 150^\circ$ were omitted because of lower statistical quality, and those at -60° because of detector problems. The data for the different groups were combined with a flux-weighting technique. The measured differential cross section is reduced to the total structure factor $S(Q)$ according to the Faber-Ziman definition:

$$\frac{d\sigma}{d\Omega} = \langle \bar{b} \rangle^2 [S(Q) - 1] + \langle \bar{b}^2 \rangle, \quad (1)$$

where $\langle \bar{b} \rangle = \sum_i x_i \bar{b}_i$ and $\langle \bar{b}^2 \rangle = \sum x_i \bar{b}_i^2$, x_i is the atom fraction, and \bar{b}_i and \bar{b}_i^2 are the mean and mean-square

scattering amplitudes for element i averaged over the nuclear isotopes and spins for that element. $S(Q)$ as defined in Eq. (1) has the property that $S(Q) \rightarrow 1$ as $Q \rightarrow \infty$, which was used to obtain the final absolute normalization of the results.

The real-space functions complement the reciprocal-space information. The pair distribution function $g(r)$ and the radial distribution function $n(r)$ can be derived by using a Fourier transform or the method of maximum entropy. Details on the technical refinements needed to accurately derive $g(r)$ and $n(r)$ are described elsewhere.²² The following equations were used to calculate these quantities:

$$D(r) = \frac{2}{\pi} \int_0^{Q_{\max}} [S(Q) - 1] \sin(Qr) Q dQ, \quad (2)$$

$$g(r) = D(r) / 4\pi r \rho_0 + 1, \quad (3a)$$

and

$$n(r) = rD(r) + 4\pi r^2 \rho_0, \quad (3b)$$

where ρ_0 is the total number density and $Q_{\max} \leq 20 \text{ \AA}^{-1}$.

Figures 1(a)–1(d) show the total structure factors for APb alloys ($A = \text{Na, K, Rb, and Cs}$) measured at temperatures above their melting points. The KPb data obtained previously² were reanalyzed with the procedures used for the data reported here. For comparison, the structure factor of KPb measured by Reijers *et al.*^{1,23} is also included in Fig. 1(b) (solid circles). Figures 2(a)–2(d) show the radial distribution functions $n(r)$ obtained by Fourier transform of $S(Q)$. Contrary to our previous analysis of data on KPb,² we have chosen not to use the Lorch modification or any other modification function in the Fourier transformation. The solid and dashed lines in Figs. 1 and 2 represent model calculations, which will be discussed in Sec. III. The values for the liquid density of these alloys are tabulated in Table III. For NaPb and KPb, they are taken from measurements by Hesson

TABLE II. Anisotropic Debye-Waller factors. The Debye-Waller factors have the general form $\exp[-2\pi^2(U_{11}h^2a^{*2} + \dots + 2U_{23}klb^*c^*)]$.

Parameter	NaPb (370 K)	KPb (RT)	RbPb (RT)	CsPb (RT)
$A(1), U_{11}$	0.058(7)	0.056(3)	0.040(3)	0.040(4)
$A(1), U_{22}$	0.085(7)	0.042(2)	0.029(2)	0.048(3)
$A(1), U_{33}$	0.139(10)	0.015(2)	0.050(3)	0.039(4)
$A(1), U_{12} = U_{13}$	0.0	0.0	0.0	0.0
$A(1), U_{23}$	0.040(6)	0.000(2)	0.001(2)	0.007(3)
$A(2), U_{11} = U_{22}$	0.117(6)	0.050(2)	0.038(2)	0.048(3)
$A(2), U_{33}$	0.070(8)	0.019(2)	0.033(2)	0.031(3)
$A(2), U_{12}$	0.030(8)	-0.006(3)	-0.001(2)	0.009(4)
$A(2), U_{13} = -U_{23}$	0.002(4)	0.008(1)	0.003(1)	-0.009(2)
Pb, U_{11}	0.061(3)	0.040(1)	0.031(1)	0.037(2)
Pb, U_{22}	0.066(3)	0.036(1)	0.030(1)	0.031(2)
Pb, U_{33}	0.068(3)	0.023(1)	0.028(1)	0.028(2)
Pb, U_{12}	0.000(1)	0.003(1)	0.003(1)	-0.002(1)
Pb, U_{13}	-0.015(2)	-0.008(1)	-0.008(1)	-0.004(1)
Pb, U_{23}	0.031(1)	0.005(1)	0.010(1)	0.009(1)

*et al.*²⁴ and Saar and Ruppertsberg,²⁵ which indicate an appreciable volume contraction of 17% and 26%, respectively. For RbPb and CsPb, where no measurements are available, the values for the densities were estimated from our present measurements using the low- r part of $D(r)$. The values thus derived show a volume contraction of

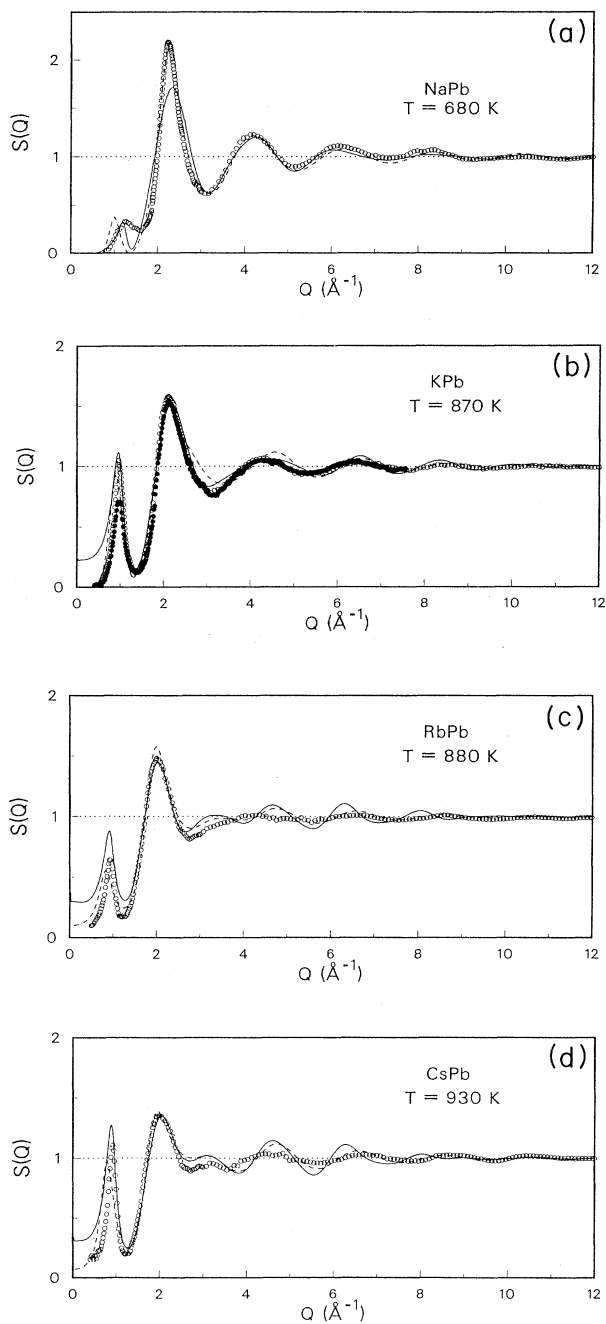


FIG. 1. Total structure factors for NaPb, KPb, RbPb, and CsPb. The points refer to the experimental results; the solid line to the calculations according to the RPSU model; and the dashed line to the RISM. The parameters used in these calculations are shown in Table IV.

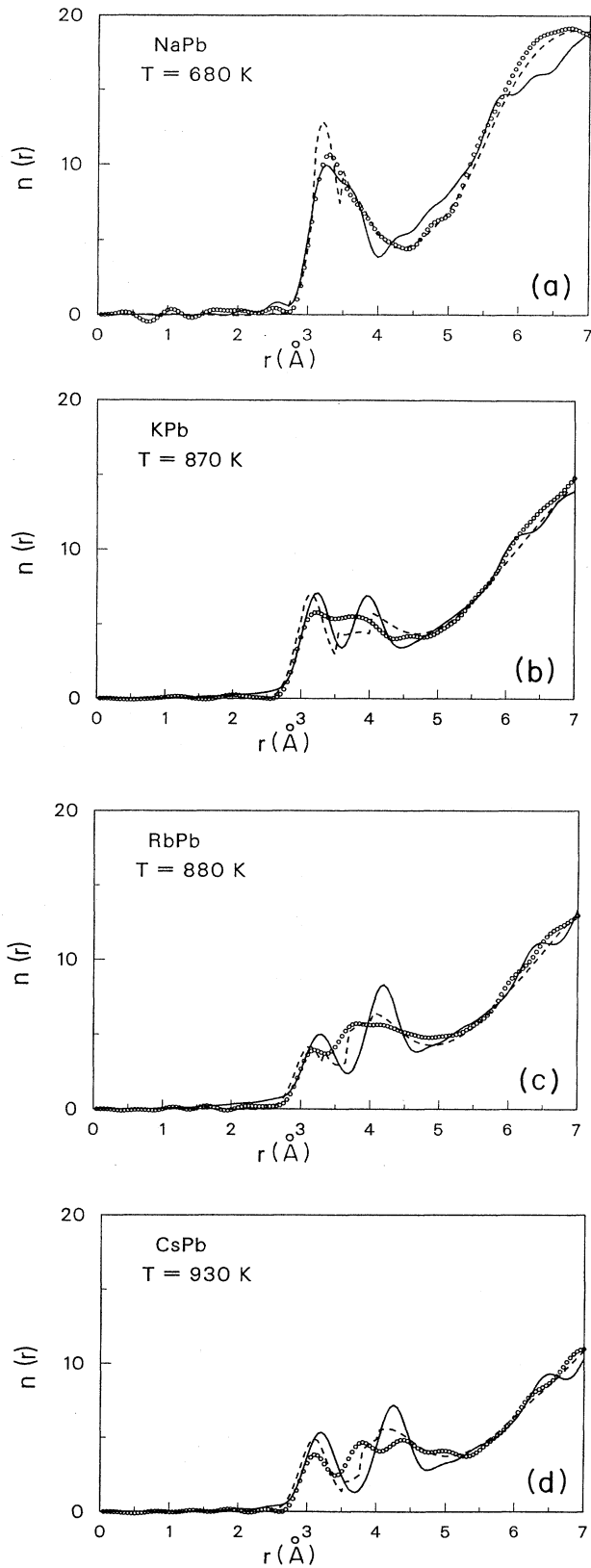


FIG. 2. Radial distribution function $n(r)$ for NaPb, KPb, RbPb, and CsPb. Notation same as in Fig. 1.

TABLE III. Structural data for liquid APb alloys.

	NaPb 680 K	KPb 870 K	RbPb 880 K	CsPb 930 K
Number density ρ_0 (\AA^{-3})				
Liquid	0.0308 ^a	0.0217 ^b	0.0199 ^c	0.0168 ^c
Solid	0.0322	0.0255	0.0233	0.0213
$S(Q)$ peak positions (\AA^{-1})				
First peak	1.25 1.25 ^e	0.96 0.97 ^f	0.93	0.92
Second peak	2.24	2.11 2.11 ^f	2.01	2.01
$T(r)$ peak positions (\AA)				
First peak	3.27	3.17	3.16	3.15
Second peak	3.7 ^g	3.70	3.73	3.75
Third peak				4.40

^aReference 19.

^bReference 20.

^cEstimated from $D(r)$, present work.

^dFrom Table I.

^eFrom Ref. 26; note that the temperature was 693 K.

^fFrom Ref. 23.

^gUnresolved peak.

35% relative to the component liquid metals, which is consistent with the behavior of NaPb, KPb, and other alloys with comparable electrical and thermodynamic properties.

The total structure factors of APb shown in Fig. 1 exhibit a characteristic FSDP at low wave vectors. For NaPb, the position of the FSDP at 1.25\AA^{-1} is identical to that reported by Takeda *et al.*²⁶ For KPb, its position at 0.96\AA^{-1} agrees with values reported by Reijers *et al.*²³ This position remains unaltered within experimental uncertainties as a function of composition while its height varies strongly. In the Na-Pb alloy, a departure from the equiatomic composition leads to an increase in height, with the maximum reached at Na₄Pb.²⁶ In K-Pb, the magnitude of FSDP is maximum at the equiatomic composition.²³ The temperature dependence of the FSDP has been studied earlier in KPb (Ref. 2) and more recently in CsPb (Ref. 27), where an increase in temperature produced a significant decrease in the magnitude and an insignificant change in the position.

From the present work, the position of the first peak in $S(Q)$ appears to be affected by the alkali metal, but not in a systematic fashion. As shown in Table III, the Q coordinate changes abruptly from NaPb to KPb and very little in going from KPb to RbPb and CsPb; this experimental finding raises a question as to whether the first peak in NaPb could be interpreted by similar arguments as used for KPb, RbPb, and CsPb. This question will be discussed later. However, it is clear that the presence of this first peak has important structural implications related to ordering in these alloys. The changes in the magnitude of the first peak height should be studied in connection with the contrast between the alkali metals on the one hand and Pb on the other. The increase from Na to K represents a real change in the structure, while the decrease from K to Rb and increase to Cs reflect, at least

partially, the changes in the scattering length of the alkali metal.

The positions of the second peak in $S(Q)$ follow the same trend as for the FSDP; its magnitude decreases on going from Na to Cs and is not as strongly affected by temperature.² At high wave vectors, a loss in structure is evident as one goes from Na to Cs.

Information about the real-space structure can be obtained from either function, $g(r)$ or $n(r)$. We have chosen to show $n(r)$ in Figs. 2(a)–2(d). Most of the structural information can be derived from the *first coordination shell*, which extends from about 2.5\AA to the onset of the steep rise starting around 4.5\AA for NaPb and KPb and around 5\AA for RbPb and CsPb. A second coordination shell is present and is centered around 6.5 – 7\AA , which is not visible in all the figures. In what follows, we will focus exclusively on the first coordination shell.

The positions of the peaks located in the first coordination shell have been estimated by least-squares-fitting Gaussian functions to the data for $T(r) = 4\pi\rho_0 r g(r)$, which is an appropriate procedure since the broadening in r space due to truncation of the data at Q_{\max} enters symmetrically in $T(r)$. The effect of the truncation at Q_{\max} was taken into account. The values obtained are listed in Table III.

Except for NaPb, the first coordination shell is characterized by the presence of two or more maxima. This fact can be taken as evidence for the existence of clusters of atoms: in simple alloys where free atoms exist, only one maximum is usually detected. In the case of NaPb, the single asymmetric peak is tentatively fitted by two unequal Gaussians.

By analogy with the crystal data, the first peak in KPb, RbPb, and CsPb can be assigned to the Pb-Pb distance in the liquid within the $A_4\text{Pb}_4$ structural unit and gives strong evidence for the survival of these units into the

liquid state. The fact that this Pb-Pb distance is slightly larger than the intratetrahedral Pb-Pb distance observed in the crystal reflects the effects of melting. The second peak can be assigned to A-Pb within the same structural unit. In RbPb, this second peak is not as well defined as in CsPb and covers a rather flat shoulder extending to about 4.5 Å; it is possible that a third peak could exist as in CsPb. The third peak clearly exhibited in CsPb is difficult to assign to a specific interaction; interestingly, it exists at all the different liquid temperatures measured.²⁷ The $n(r)$ deduced from room-temperature structure measurements on CsPb shows only two peaks. The third peak is undoubtedly a liquid signature, and if one takes into consideration the scattering contrast, it could be related to an A-Pb distance where the alkali-metal and the Pb atoms are in a different arrangement than in a tetrahedron. Finally, in NaPb, since the Pb-Pb and Na-Pb distances exhibited in Table I differ by only a few tenths of an angstrom, it is plausible that the first coordination shell in the liquid consists of two unresolved peaks.

Based on the above interpretation, a partial coordination number $Z(ab)$ representing the average number of b atoms about an a atom in the first coordination shell, where a and b refer to either A or Pb, can be calculated by converting the fitted Gaussians to $n(r)$ form. However, the area calculated under each peak in $n(r)$ was largely affected by the number of peaks specified and by the starting parameters assigned in the nonlinear least-squares fitting. Thus, the coordination numbers $Z(ab)$ deduced from each peak and assigned to Pb-Pb (first peak) and to A-Pb (second and subsequent peaks) have rather large numerical uncertainties. To summarize these results, $Z(\text{PbPb})$ varies from ~ 3.6 in NaPb to ~ 2 in KPb, RbPb, and CsPb; this number should be viewed as an average coordination number, reflecting the presence of tetrahedrally arranged Pb atoms and other higher (in NaPb) or lower (in the other compounds) coordinated Pb atoms; $Z(\text{PbPb})=3$ for isolated tetrahedra. This is in consonance with a thermodynamical interpretation of the heat-capacity data, where it is suggested that the $A_4\text{Pb}_4$ entities are dissociating to form dimers and/or free atoms as the temperature increases above the melting point. In accord with this suggestion, a decrease in $Z(\text{PbPb})$ was observed with increasing temperature in the case of CsPb.²⁷ Within the numerical uncertainties, a small decrease in $Z(\text{PbPb})$ was obtained as the alkali metal changes from K to Rb and to Cs. A value of 3 was obtained for $Z(\text{PbPb})$ from the analysis of the room-temperature measurements.

3. Liquid dynamics in KPb

The data collected from inelastic neutron diffraction on KPb were corrected to scattering function form, $S(\phi, E)$, and then to constant Q form, $S(Q, E)$, using a cubic spline interpolation.¹⁴ As an initial check, the structure factor $S(Q)$ was calculated from the data using the relation

$$S_{\Delta}(Q) = \int_{-\Delta}^{\Delta} S(Q, E) dE. \quad (4)$$

For $\Delta \rightarrow \infty$, this should reduce to the structure factor

measured in the diffraction measurement, neglecting errors due to inelasticity in the latter case and experimental errors such as multiple scattering in both cases. Further, while both structure factors should be normalized so that $S(Q) \rightarrow 1$ as $Q \rightarrow \infty$, incoherent scattering is included in the inelastic results, but not in the diffraction results, with the definitions used in the present analysis. Figure 3 compares the SEPD results for liquid KPb with $S_{\Delta}(Q)$ obtained from the inelastic scattering with $\Delta=40$ and 5 meV, respectively. The first case represents the closest approach to $S(Q)$ possible in this measurement, i.e., the instantaneous ($t=0$) density correlations in the structure, while the second gives a measure of the contributions from low-energy transfers, representing the long-time average of the structural correlations. The agreement between the inelastic results for $\Delta=40$ meV and the diffraction result is reasonable, considering the lower Q resolution inherent in the inelastic measurements and the very different experimental procedures. The shoulder on the right side of the main peak and the splitting of the third peak in $S_{\Delta}(Q)$ may represent experimental errors in the detector normalization. The FSDP at $Q=1 \text{ \AA}^{-1}$ shows up clearly in the inelastic measurements at both values of Δ , indicating that the structural correlations responsible for this peak persist for times as long as $t = \hbar/\Delta \approx 10^{-13}$ sec and possibly longer. This upper limit could be extended with a higher-resolution measurement.

The scattering function $S(Q, E)$ for the solid phase consists of an elastic peak and inelastic spectra for positive and negative values of E . For the liquid, the inelastic spectrum is essentially unchanged, but the elastic peak is broadened into a quasielastic one by atomic diffusion. The full width at half maximum, $\Gamma(Q)$, of this peak was obtained for different values of Q by fitting a Lorentzian function

$$S_{\text{qe}}(Q, E) = \frac{1}{2\pi} \left[\frac{A\Gamma^2}{\Gamma^2 + E^2} \right], \quad (5)$$

broadened by the calculated resolution function,²⁸ to the quasielastic region of each constant- Q spectrum. Figure

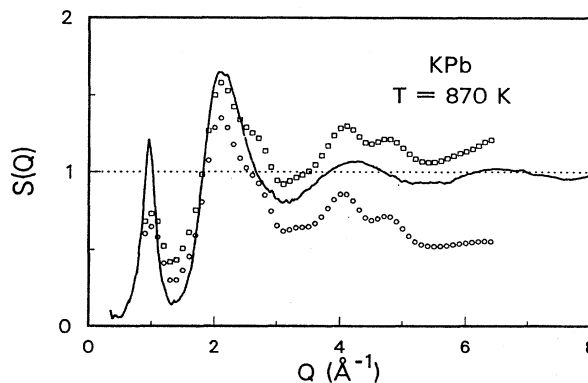


FIG. 3. Structure factors $S(Q)$ for liquid KPb. Solid line, $S(Q)$ from diffraction measurement. Points, $S_{\Delta}(Q) = \int_{-\Delta}^{\Delta} S(Q, E) dE$ from inelastic scattering measurements: \square , $\Delta=40$ meV; \circ , $\Delta=5$ meV.

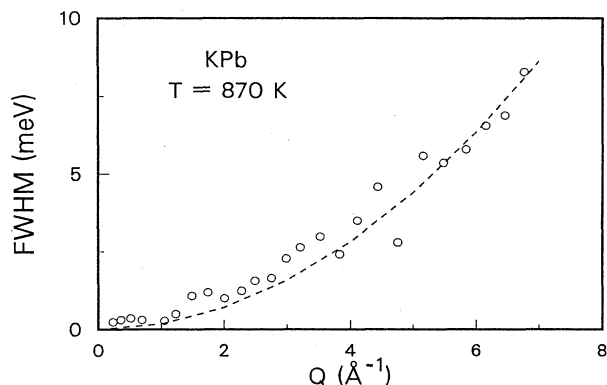


FIG. 4. Full width at half maximum of the quasielastic scattering as a function of Q . Circles, experimental data; dashed line, $\Gamma = 2\hbar DQ^2$ with $D = 1.2 \times 10^{-5}$ cm²/sec.

4 shows the results for $\Gamma(Q)$. The dashed line represents the best fit of the form expected for simple diffusion,

$$\Gamma = 2\hbar DQ^2, \quad (6)$$

with $D = 1.2 \pm 0.2 \times 10^{-5}$ cm²/sec. This is somewhat lower than the value observed in pure liquid lead,²⁹ $D = 2.2 \times 10^{-5}$ cm²/sec, and may reflect a larger mass for the diffusing particles. It is substantially lower than the diffusion constants observed in liquid Li₄Pb,³⁰ 6.0×10^{-5} cm²/sec.

An energy distribution function $G(E)$ for the inelastic scattering in the liquid was obtained by averaging the function

$$G(Q, E) = [S(Q, E) - S_{qc}(Q, E)] \left[\frac{2\overline{ME}}{\hbar^2 Q^2} \right] \times [1 - \exp(-E/k_B T)] \quad (7)$$

over the measured values of Q . The result, plotted in Fig. 5, is a slowly varying function of E with a broad maximum around 9 meV but no sharp peaks that can be ascribed to vibrations of a molecular character. Such

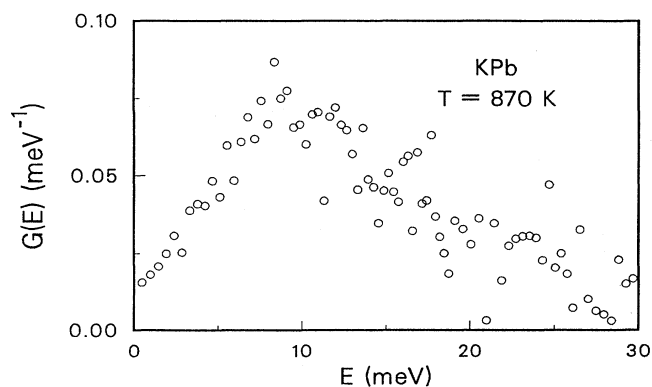


FIG. 5. Q -averaged energy distribution function for the inelastic scattering.

modes may be present but contributing with an intensity that is too low to be observed against the background of translational motions. Another possible explanation, in terms of a limited lifetime for the molecular units, seems to be ruled out by the relatively long lifetimes associated with the FSDP, as discussed above. The form of the spectrum in Fig. 5 is, in fact, qualitatively similar to that observed in liquid lead.³¹ The equivalent spectrum for the solid K Pb did not show any evidence for molecular vibrations either. A Raman scattering measurement on the solid also failed to show any significant vibrational peaks,³² although vibrational modes have been observed in NaSi and KGe.³³

III. STRUCTURAL MODELS

The value of information derived from structural measurements can be considerably enhanced if one can build a model or theory capable of accurately representing the key features of, e.g., the total structure factor. Specifically, in a binary system, such a model provides the partial structure factors and partial pair distribution functions that play a vital role in our understanding of the liquid. For cases such as those studied here, where an FSDP is present, questions to be addressed include what is the physical meaning of the FSDP, which partial structure factors contribute to its presence, and what geometrical correlations are implied? The real-space functions can also be decomposed into the partial functions within the framework of a model and are essential in assessing preferential coordination and the nature of ordering in the liquid. For the alkali-metal-lead alloys, such an approach must be employed since it is impossible to experimentally derive the partial function because there are no suitable isotopes for the substitution method, which has been used so successfully in certain molten salts and alloys. In this section, we will report the results obtained by applying the random packing of structural units (RPSU) model and the reference interaction site model (RISM). Both models use structural units from the solid, e.g., the A_4Pb_4 species.

In the case of the RPSU model,³⁴ which was originally developed by Egelstaff *et al.*,³⁵ the structural units are distributed according to a random packing of hard spheres. The structure factor is expressed as

$$S(Q) = f_1(Q) + f_2(Q)[S_c(Q) - 1] + 1 - \langle \bar{b}^2 \rangle / \langle \bar{b} \rangle^2, \quad (8)$$

where $f_1(Q)$ is the form factor of the structural unit, $f_2(Q)$ is another form factor expressing the correlation between two distinct units, and $S_c(Q)$ is the Percus-Yevick solution for the random packing of hard spheres. To evaluate $f_2(Q)$, a physical assumption about the correlation between orientations of different structural units must be made.³⁵ In the present calculations, the orientations were taken to be random and uncorrelated. Following Ref. 2, the structural unit was defined to be A_4Pb_4 and consisted of a Pb_4 tetrahedron surrounded by a larger A_4 tetrahedron oppositely directed. The coordinates were derived from the crystal structures described

in the previous section. A slight expansion (1–3 %) of the unit was applied to bring the leading edge of the first peak in $n(r)$ calculated from the model into line with the experimental value, except in the case of NaPb, where the crystallographic data were taken at high temperature (Table I). Only two additional parameters are needed: the hard-sphere diameter and the packing fraction $\eta (= \pi \sigma^3 \rho_0 / 6n)$, where n is the number of atoms in the structural unit). A Debye-Waller factor, $\exp(-Q^2 \langle u^2 \rangle / 2)$, where $\langle u^2 \rangle$ is the mean-square fluctuation in bond distances within the structural unit, is applied to give approximately the correct damping of oscillations in $S(Q)$ at high Q . The calculated structures for NaPb, KPb, RbPb, and CsPb are plotted in Fig. 1 along with the experimental results. The numerical values used for σ , η , ρ_0 , and $\langle u^2 \rangle$ are shown in Table IV.

In the case of RISM, which was first proposed by Andersen and Chandler,³⁶ we have utilized a numerical procedure developed by Lowden and Chandler.³⁷ RISM has been applied to a variety of molecular liquids ranging from liquid CCl₄ to CS₂, C₆H₆,³⁸ SbCl₃,³⁹ and very recently GeBr₄.⁴⁰ The representation of the structure factors by RISM has been satisfactory, except in the case of liquid SbCl₃ and GeBr₄, where the correspondence between calculations and experiments remained qualitative. The structure factor is expressed as

$$S(Q) = \sum_{\alpha\gamma} \bar{b}_\alpha \bar{b}_\gamma [w_{\alpha\gamma}(Q) + \rho_m h_{\alpha\gamma}(Q) - \delta_{\alpha\gamma}] / n \langle \bar{b} \rangle^2 + 1, \quad (9)$$

where ρ_m is the density of structural units, $h_{\alpha\gamma}$ is the Fourier transform of the pair correlation function between sites α and γ of different units, and $w_{\alpha\gamma}$ is that between sites α and γ of the same unit. If $d_{\alpha\gamma}$ is the equilibrium distance between sites α and γ in the same structural unit, and $\Delta d_{\alpha\gamma}$ is the root-mean-square derivation in $d_{\alpha\gamma}$, the vibration of the atoms around their equilibrium position is included in $w_{\alpha\gamma}$:

$$w_{\alpha\gamma}(Q) = \frac{\sin(Qd_{\alpha\gamma})}{Qd_{\alpha\gamma}} \exp[-1/2(Q\Delta d_{\alpha\gamma})^2]. \quad (10)$$

As in the case of the RPSU model, the structural unit

TABLE IV. Parameters for liquid APb alloys used in model fits.

Parameter	NaPb	KPb	RbPb	CsPb
	RPSU model			
σ (Å)	5.4	6.4	6.8	7.0
η	0.45	0.37	0.40	0.38
ρ_0 (10 ²⁴ cm ⁻³)	0.0437	0.0216	0.0194	0.0169
$\langle u^2 \rangle^{1/2}$ (Å)	0.15	0.2	0.2	0.2
	RISM model			
σ_A (Å)	2.7	3.0	3.3	3.5
σ_{Pb} (Å)	3.5	4.0	4.0	4.0
ρ_0 (10 ²⁴ cm ⁻³)	0.0308	0.0216	0.0192	0.0168
Δd_{AA} (Å)	0.3	0.4	0.4	0.4
Δd_{PbPb} (Å)	0.15	0.2	0.2	0.2
Δd_{APb} (Å)	0.3	0.4	0.4	0.4

was taken to be A_4Pb_4 , consisting of an A tetrahedron surrounding a Pb tetrahedron. The positions of the atoms were taken from Table I; the values of the hard-sphere radii of the alkali-metal atoms and Pb were reasonably optimized to give the best fit to the data. The parameters used in the calculations are given in Table IV, and results are plotted in Fig. 1. The correspondence between the measurements and calculations with the RPSU model and RISM is satisfactory for all the systems that we have studied.

For NaPb [Fig. 1(a)], the FSDP is better represented by the RPSU model, but the density needed was 40% higher than the measured one. An FSDP is obtained from RISM, but its position is quite different from the experimental one. Both models exaggerate the minimum that follows the FSDP and, consequently, give a rather poor representation of the low- Q section of the structure factor. In an effort to improve the correspondence, we tried other structural units, such as Na₄Pb, Pb₄, or Na₄Pb₄ with additional free Na and Pb atoms; the fits obtained were not improved. (Na₄Pb was introduced since in Na-Pb an "octet" compound, Na₄Pb, is present and interesting features in the thermodynamic and transport properties are reported at both 4:1 and 1:1 compositions.) The main peak height and width are much better reproduced by RISM than by the RPSU model. Interestingly, when identical orientations are imposed, the RPSU-model calculations give an excellent representation of the main peak. The remaining features are equally well reproduced by either model. In real space, both models lead to a double peak in the first coordination shell, the first one located at ~ 3.25 Å and the second at ~ 3.5 Å, which correspond to the crystalline Pb-Pb and Na-Pb distances, respectively (Table I). The minimum calculated from RISM reproduces very well the measurements, while the RPSU gives a better fit for the maximum.

In the case of KPb, in addition to the IPNS data, we have plotted the experimental results obtained by Reijers *et al.*¹ using the Petten reactor [closed circles in Fig. 1(b)]. The RPSU model reproduces the IPNS measurements slightly better than RISM. The differences between the two sets of experimental data, especially those at low Q , are not fully resolved, but the inherent difference in resolution between a pulsed-source instrument and a reactor instrument may be an important factor.⁴¹ Finally, for the RbPb and CsPb alloys, both calculations tend to overemphasize the high- Q structure with well-pronounced peaks, while the experiments show a rather damped oscillatory behavior. At low Q , the FSDP and the main peak are satisfactorily represented.

In real space, the calculated $n(r)$ functions exhibit two peaks whose positions are in agreement with the measurements (Fig. 2); the minimum is better reproduced by RISM. It should be noted that the parameters in both models were chosen to give the best fit in reciprocal space rather than in real space. The three-peak structure obtained experimentally in CsPb is not explained by either model.

At this point, a conclusion can be reached from the calculations presented here and many others that we have carried out. The introduction of correlations in the

orientations of the structural units inherent in RISM does not represent any significant advantage since the RPSU model works remarkably well, with the exception of the main peak in NaPb. The assumption that the structural unit is A_4Pb_4 leads to a reasonable representation of the results. Other structural units were tried, such as a Pb_4 tetrahedron and A_8Pb_8 and $A_{16}Pb_{16}$ units. The Pb_4 tetrahedron gives an FSDP in $S(Q)$, but the main peak is poorly represented, while the larger structural units worsen the agreement between model and experiment. The fact that, for the liquids studied here, both models led to an overall satisfactory representation of the data can be explained by taking into account that the A_4Pb_4 units are almost spherical (except in the case of NaPb); as a result, the correlations in orientations between different units do not play an important role. In one recent study of haloaluminates where the prevalent structural units are highly anisotropic, a pronounced difference was obtained between the two models.⁴²

Partial structure factors S_{ab} can be calculated from these models, although they are not accessible experimentally. The partial structure factors for CsPb, defined according to Faber and Ziman, derived from both models are given in Fig. 6. In Fig. 7, we show the Bhatia-Thornton⁴³ structure factors defined as

$$S_{NN}(Q) = c_1 S_{11}(Q) + c_2 S_{22}(Q) + 2(c_1 c_2)^{1/2} S_{12}(Q), \quad (11)$$

$$S_{CC}(Q) = c_1 c_2 [c_2 S_{11}(Q) + c_1 S_{22}(Q) - 2(c_1 c_2)^{1/2} S_{12}(Q)],$$

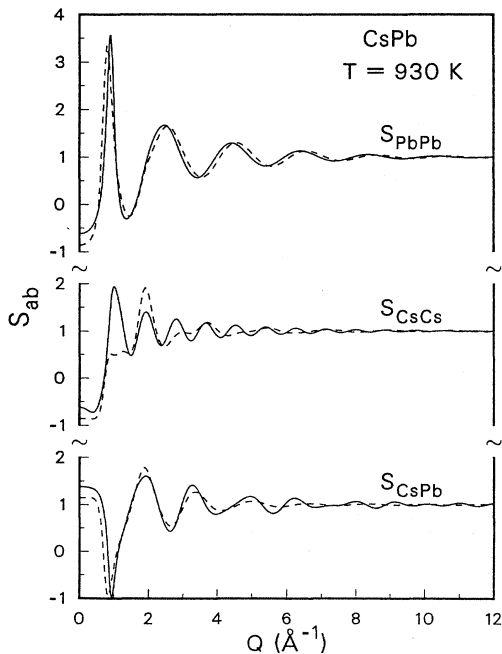


FIG. 6. Partial structure factors S_{PbPb} , S_{CsCs} , and S_{CsPb} , according to the RPSU (solid line) and RISM (dashed line) models.

and

$$S_{NC}(Q) = c_1 c_2 [S_{11}(Q) - S_{22}(Q) + (c_2 - c_1) S_{12}(Q) / (c_1 c_2)^{1/2}].$$

$S_{NN}(Q)$ and $S_{CC}(Q)$ correspond to the mean-square fluctuation

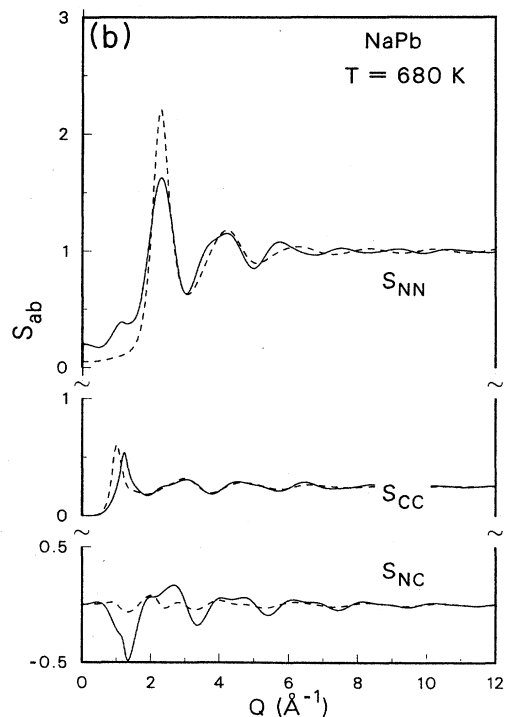
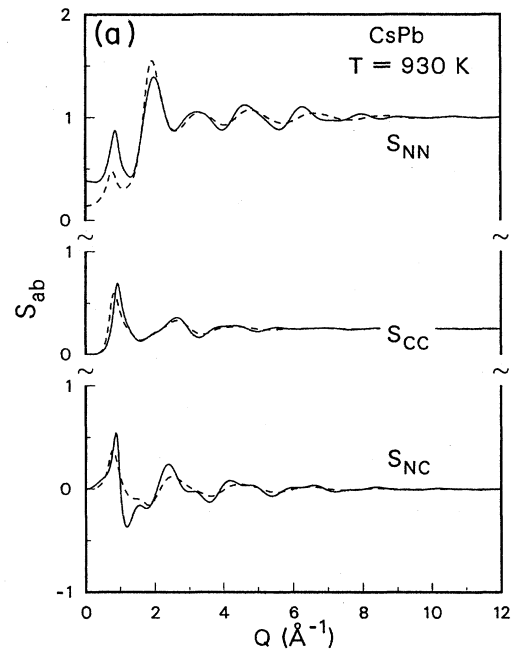


FIG. 7. Bhatia-Thornton structure factors $S_{CC}(Q)$, $S_{NN}(Q)$, and $S_{NC}(Q)$ for (a) CsPb and (b) NaPb derived from the RPSU (solid line) and RISM (dashed line) models.

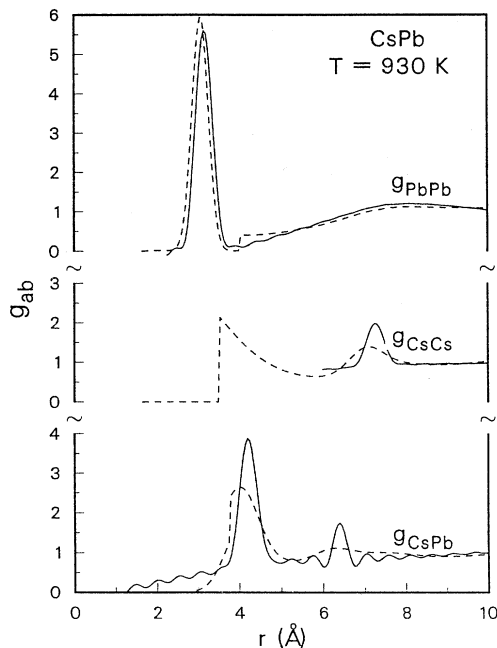


FIG. 8. Pair radial distribution functions, g_{PbPb} , g_{CsCs} , and g_{CsPb} , according to the RPSU (solid line) and RISM (dashed line) models.

tuations in the number density and concentration, respectively, while S_{NC} is a cross term. As shown in Fig. 7(a) for CsPb, all three structure factors contribute to the FSDP. This is in contrast to the situation in most liquid alloys and molten salts where the prepeak shows up in S_{CC} only.⁴⁴ The main peak in the total structure factor at about 2 \AA^{-1} derives mainly from S_{NN} . Figure 7 shows the Bhatia-Thornton structure factors for NaPb. Here, the FSDP is given primarily by S_{CC} , with only a small contribution from S_{NN} for the RPSU model and none for RISM. This provides further indication that the FSDP has a different character in NaPb compared with the other APb alloys.

In real space, both models give a satisfactory representation of the data. Of particular interest are the partial radial distribution functions. Figure 8 shows the partial pair correlation functions $g_{ab}(r)$ for CsPb calculated from the two models. The discontinuities in the RISM curve are, of course, due to the hard-sphere potentials used in the calculations. The presence of a remarkably sharp main peak in g_{PbPb} with a very low value for the minimum arises from the Pb tetrahedra.

Very recently, molecular-dynamics simulation of liquid KPb has been carried out by Hafner,⁴⁵ using concentration-dependent ionic pseudopotentials taking

account of a finite electron mean free path. Strong Pb-Pb correlations are observed, with a coordination number of about 3.5 Pb atoms about an average Pb atom and angular distributions consistent with a high concentration of Pb_4 tetrahedra. A peak is observed in $S(Q)$ at small Q , but displaced to higher Q , smaller and poorly separated from the rest of the diffraction pattern compared with the experimental data. To our knowledge, this is the only attempt that has been made to model these liquids on the basis of interatomic potentials.

IV. CONCLUSION

In this paper, structural results are presented for the alkali-metal-lead alloys at the equiatomic composition showing evidence of intermediate-range order. A remarkable FSDP is present at low wave vectors, $Q \sim 1 \text{ \AA}^{-1}$. Its presence can be shown to be related to structural units, $A_4\text{Pb}_4$, similar to those in the intermetallic solid compounds. These have been used to construct structural units within the framework of two models for the liquid structures, the RPSU model and RISM. The calculations give a satisfactory representation of the experiments with physically meaningful values for the different parameters. In contrast to the diffraction results for the FSDP and to the energy dependence of the scattering associated with the FSDP, which suggests a relatively long lifetime for the structural units, no evidence for vibrations of a molecular character was observed in the inelastic scattering. Higher-energy resolution studies may resolve this contradiction. Finally, it is hoped that, in the future, direct measurements of the partial structure factors will be achieved by other experimental means, for example, anomalous x-ray scattering.

ACKNOWLEDGMENTS

We wish to thank R. Kleb for installation and calibration of the furnace for the inelastic measurements, and the operations staff at the Intense Pulsed Neutron Source at Argonne National Laboratory for assistance with the neutron experiments. The preparation of the vanadium holders and the electron-beam welding was carefully carried out by C. Konicek. We kindly acknowledge Dr. P. G. O'Hare for the use of his glovebox, Dr. M. Blander for a critical reading of the manuscript, and Dr. M. Grimsditch for performing Raman scattering on solid KPb. This work was supported by the U.S. Department of Energy, Division of Materials Sciences, Office of Basic Energy Sciences, under Contract No. W-31-109-ENG-38. H. T. J. Reijers gratefully acknowledges the support of the Stichting voor Fundamenteel Onderzoek der Materie, The Netherlands.

*On leave from the Solid State Physics Laboratory, University of Groningen, The Netherlands.

¹H. T. J. Reijers, W. van der Lugt, and C. van Dijk, *Physica B+C* **144B**, 404 (1987).

²M.-L. Saboungi, R. Blomquist, K. J. Volin, and D. L. Price, *J. Chem. Phys.* **87**, 2278 (1987).

³J. A. Meijer, W. Geertsma, and W. van der Lugt, *J. Phys. F* **15**, 899 (1985); J. A. Meijer, W. van der Lugt, and G. J. B. Vinke,

- ibid.* **16**, 845 (1986).
- ⁴C. van der Marel, A. B. van Oosten, W. Geertsma, and W. van der Lugt, *J. Phys. F* **12**, 2349 (1982); W. F. Calaway and M.-L. Saboungi, *ibid.* **13**, 1213 (1983).
- ⁵S. Matsunaga, T. Ishiguro, and S. Tamaki, *J. Phys. F* **13**, 587 (1983); M.-L. Saboungi, S. J. Herron, and R. Kumar, *Ber. Bunsenges. Phys. Chem.* **89**, 375 (1985).
- ⁶G. K. Johnson and M.-L. Saboungi, *J. Chem. Phys.* **86**, 6376 (1987); M.-L. Saboungi, H. T. J. Reijers, M. Blander, and G. K. Johnson, *ibid.* **89**, 5869 (1988).
- ⁷M.-L. Saboungi, S. R. Leonard, and J. Ellefson, *J. Chem. Phys.* **85**, 6072 (1986).
- ⁸P. J. Tumidajski, A. Petric, T. Takenake, M.-L. Saboungi, and A. D. Pelton, *J. Phys. F* (to be published).
- ⁹E. Busmann, *Z. Anorg. Allg. Chem.* **313**, 90 (1961).
- ¹⁰J. D. Jorgensen and J. Faber, Argonne National Laboratory Report No. ANL-82-80, 1983, p. 105.
- ¹¹U. Walter, D. L. Price, S. Susman, and K. J. Volin, *Phys. Rev. B* **37**, 4232 (1988).
- ¹²D. L. Price, J. M. Carpenter, C. A. Pelizzari, S. K. Sinha, I. Bresof, and G. E. Ostrowski, Argonne National Laboratory Report No. ANL-82-80, 1983, p. 207.
- ¹³D. L. Price and J. R. D. Copley, *Phys. Rev. A* **11**, 2124 (1975).
- ¹⁴C.-K. Loong and D. L. Price (unpublished).
- ¹⁵R. E. Marsh and D. P. Shoemaker, *Acta Crystallogr.* **6**, 197 (1953).
- ¹⁶I. F. Hewaidy, E. Busmann, and W. Klemm, *Z. Anorg. Allg. Chem.* **328**, 283 (1964).
- ¹⁷V. F. Sears, in *Neutron Scattering*, Vol. 36A of *Methods of Experimental Physics*, edited by K. Sköld and D. L. Price (Academic, Orlando, 1986), p. 521.
- ¹⁸H. M. Rietveld, *J. Appl. Cryst.* **2**, 65 (1969); R. B. von Dreele, J. D. Jorgensen, and C. G. Windsor, *ibid.* **15**, 581 (1982).
- ¹⁹J. D. Jorgensen and F. J. Rotella, *J. Appl. Crystallogr.* **15**, 27 (1982).
- ²⁰F. J. Rotella (unpublished).
- ²¹J. W. Richardson, Jr. and J. Faber, Jr., *Adv. X-Ray Anal.* **29**, 45 (1985).
- ²²D. L. Price (unpublished); W. S. Howells, D. L. Price, and D. G. Montague (unpublished).
- ²³R. Reijers, W. van der Lugt, C. van Dijk, and M.-L. Saboungi, *J. Phys.: Condens. Matt.* (to be published).
- ²⁴J. C. Hesson, H. Shimotake, and J. M. Tralmer, *J. Met.* **20**, 6 (1968).
- ²⁵J. Saar and H. Ruppertsberg, *Z. Phys. Chem. Neue Folge (Lam VI Proc.)* **156**, 587 (1988).
- ²⁶S. Takeda, S. Harada, S. Tamaki, E. Matsubara, and Y. Waseda, *J. Phys. Soc. Jpn.* **56**, 3934 (1987).
- ²⁷M.-L. Saboungi, D. L. Price, R. Reijers, K. J. Volin, and W. van der Lugt (unpublished).
- ²⁸C.-K. Loong, S. Ikeda, and J. M. Carpenter, *Nucl. Instrum. Methods A* **260**, 381 (1987).
- ²⁹T. E. Farber, *An Introduction to the Theory of Liquid Metals* (Cambridge University Press, Cambridge, England, 1972), p. 164.
- ³⁰M. Soltwisch, D. Quitmann, H. Ruppertsberg, and J. B. Suck, *J. Phys. (Paris) Colloq.* **41**, C8-167 (1980).
- ³¹O. Söderström, *Phys. Rev. A* **23**, 785 (1981).
- ³²M. Grimsditch (private communication).
- ³³H. Buerger and R. Eujen, *Z. Anorg. Allg. Chem.* **394**, 19 (1972).
- ³⁴S. C. Moss and D. L. Price, in *Physics of Disordered Materials*, edited by D. Adler, H. Fritzsche, and S. R. Ovshinsky (Plenum, New York, 1985), p. 77.
- ³⁵P. A. Egelstaff, D. I. Page, and J. G. Powles, *Mol. Phys.* **20**, 881 (1971); **22**, 944 (1971).
- ³⁶H. C. Andersen and D. Chandler, *J. Chem. Phys.* **57**, 1918 (1972); D. Chandler and H. C. Andersen, *ibid.* **57**, 1930 (1972).
- ³⁷L. J. Lowden and D. Chandler, *J. Chem. Phys.* **59**, 6587 (1973).
- ³⁸L. J. Lowden and D. Chandler, *J. Chem. Phys.* **61**, 5228 (1974).
- ³⁹E. Johnson, A. H. Narten, W. E. Thiessen, and R. Triolo, *Faraday Disc. Chem. Soc.* **66**, 287 (1978).
- ⁴⁰K. F. Ludwig, Jr., W. K. Warburton, L. Wilson, and A. I. Bienenstock, *J. Chem. Phys.* **87**, 604 (1987); K. F. Ludwig, Jr., L. Wilson, W. K. Warburton, and A. I. Bienenstock, *ibid.* **87**, 613 (1987).
- ⁴¹See, for example, F. J. Bermejo, J. C. Dore, W. S. Howells, P. Chieux, and E. Enciso, *Physica B+C* **156+157B**, 154 (1989).
- ⁴²M.-L. Saboungi, D. L. Price, K. J. Volin, K. Calkins, and R. Reijers (unpublished).
- ⁴³For a summary of various definitions of structure factors, the reader is referred to Y. Waseda, *The Structure of Non-Crystalline Materials, Liquids and Amorphous Solids* (McGraw-Hill, New York, 1980).
- ⁴⁴D. L. Price, S. C. Moss, R. Reijers, M.-L. Saboungi, and S. Susman, *J. Phys.: Condens. Matt.* **1**, 1005 (1989).
- ⁴⁵J. Hafner, *J. Phys.: Condens. Matt.* **1**, 1133 (1989).